Erschienen in: Angewandte Chemie International Edition ; 56 (2017), 14. - S. 4042-4046
https://dx.doi.org/10.1002/anie.201610275

Alignment of Amorphous Iron Oxide Clusters: A Non-Classical Mechanism for Magnetite Formation

Shengtong Sun, Denis Gebauer, and Helmut Cölfen**

Abstract: *Despite numerous studies on the nucleation and crystallization of iron (oxyhydr)oxides, the roles of species developing during the early stages, especially primary clusters and intermediate amorphous particles, are still poorly understood. Herein, both ligand-free and ligand-protected amorphous iron oxide (AIO) clusters (< 2 nm) were synthesized as precursors for magnetite formation. Thermal annealing can crystallize the clusters into magnetite particles, and AIO bulk phases with domains of pre-aligned clusters are found to be direct precursors to crystals, suggesting a non-classical aggregation-based pathway that differs from the reported oriented attachment or particle accretion mechanisms.*

Iron (oxyhydr)oxides are ubiquitous in the environment and play vital roles in many geological and biological processes, from rocks and soils to bacteria, from pigments to catalysts, from rust to magnetic nanodevices. A variety of iron (oxyhydr)oxides with distinct structures and hydrated states exist, such as hematite, magnetite, goethite, or ferrihydrite.[1] Nevertheless, despite the broad interest and great efforts from many disciplines, the detailed mechanism of iron oxide nucleation and phase transformation, and the roles of various evolved species remain obscure. Recently, it was shown that at low driving force for phase separation (i.e., low pH and iron concentration) olation polymers can be regarded as stable pre-nucleation clusters (PNCs), where the onset of oxolation within the PNCs triggers a decrease in their dynamics,[2] which is the chemical basis of a phase separation event according to the notions of the PNC pathway.[3] The mechanism is consistent with the chemistry of iron oxides that has been extensively studied for decades, where the hydrolysis of iron salts in aqueous solutions produces very small colloidal particles (also termed as polycations, clusters, or primary particles) with a size of 1–4 nm.[4] Importantly, the event of phase separation is not primarily governed by a certain critical size, but the dynamics of the clusters, based on the chemistry of the internal linkages between iron centers, which subsequently leads to aggregation, driven by the reduction of interfacial surface area. Consistently, in the recent years, there is emerging evidence that the final crystalline iron oxides are formed by the aggregation of primary particles rather than classical ion-by-ion growth modes.[5] Similar phenomena were discovered in many other systems within a common concept of particle-based non-classical crystallization.[6] Thereby, oriented aggregation or attachment (OA) is found to be a fundamental step in the formation of iron oxide crystals, such as goethite single crystals formed from ferrihydrite precursors[5a,7] and hematite spindles from the growth of akaganeite nanorods.[8] The intermediate phases with aligned nanocrystals are also known as "mesocrystals".[7a,9] Nevertheless, in the case of magnetite formation, no OA was observed, while nucleation and crystal growth occurs through rapid accretion of primary clusters with a size of approximately 1 nm along the rim of evolving nanoparticles.[5b] From the viewpoint of the PNC mechanism, this observation implies that the small growth units are nucleated nanoparticles, which contain oxolated iron centers. Thereby, in contrast to the nucleation of other minerals, such as calcium carbonate,[10] an intermediate amorphous iron oxide (AIO) bulk phase, at least larger than the primary growth unit, was not observed, although AIOs had been discovered long before.[11]

Herein, we present the first direct observation of the alignment of small amorphous clusters of less than 2 nm, before fusion into larger AIO particles and subsequent crystallization during heat-induced magnetite formation. Note that the term "oriented attachment" (OA) is avoided, as it implies the presence of nanocrystals. Moreover, as opposed to the solution case, intermediate AIO bulk phases with domains of pre-aligned clusters are observed to be direct precursors for magnetite via a solid-state phase transformation. Thus, we present the first example of iron oxide crystallization that inter-connects the important species in a non-classical crystallization pathway in a consistent manner (i.e. from clusters to amorphous intermediate particles to crystals).

AIO clusters were synthesized by the co-precipitation of Fe^{2+} and Fe^{3+} ions in ethanol via ammonia gas diffusion. Ethanol is used to kinetically stabilize the AIO clusters by preventing further oxolation and subsequent crystallization. Ethanol has proven to be effective for producing other amorphous minerals, such as calcium carbonate,[12] calcium phosphate,[13] and calcium oxalate,[14] where larger amorphous particles can be obtained. The smaller size points to the fact that the kinetic stabilization is much more effective in the case of iron oxides, suggesting that the clusters are ligated by

[*] Dr. S. T. Sun
State Key Laboratory for Modification of Chemical Fibers and Polymer Materials, College of Chemistry, Chemical Engineering and Biotechnology, Center for Advanced Low-Dimension Materials, Donghua University
Shanghai 201620 (China)
Dr. D. Gebauer, Prof. Dr. H. Cölfen
Physical Chemistry
University of Konstanz
Universitätsstrasse 10, 78457 Konstanz (Germany)
E-mail: denis.gebauer@uni-konstanz.de
helmut.coelfen@uni-konstanz.de

ethanol. Water as the solvent failed to stabilize AIO clusters and resulted in crystallites, as shown in Figure S1 in the Supporting Information. Very small clusters with a mean size of 1.7 nm were produced in ethanol (Figure 1 a–c), which are amorphous judging from selected area electron diffraction (SAED). However, without ligand protection, the AIO clusters aggregate heavily resulting in floc-like precipitates in ethanol (inset in Figure 1 a).

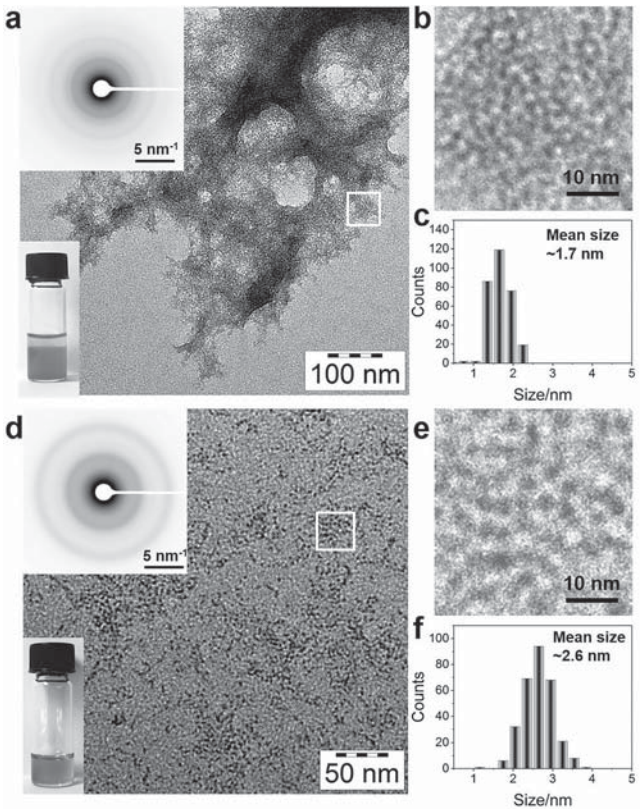

Figure 1. a) TEM image, b) enlarged view (rectangular area), and c) particle diameter distribution ($N = 300$) of ligand-free AIO clusters. The insets in (a) are the corresponding SAED pattern and a photo of a dispersion of AIO clusters in ethanol. d)–f) show ligand-protected AIO-PCDA clusters. The insets in (d) show the corresponding SAED pattern and a photo of a dispersion of AIO-PCDA clusters in toluene (1 mg mL^{-1}).

The clusters are long-term stable in ethanol and stay amorphous for more than six months. Re-dispersing the ligand-free AIO cluster flocs in water does not cause any damage or crystallization as confirmed by TEM (not shown). The addition of an amphiphilic ligand, 10,12-pentacosadiynoic acid (PCDA, chemical structure in Figure S2) leads to AIO-PCDA clusters that can be completely dispersed in organic solvents, such as toluene (inset in Figure 1 d). The AIO-PCDA clusters in toluene are also very stable for at least six months without any change and can reach very high concentrations up to 100 mg mL^{-1} at room temperature. The stabilizing mechanism of PCDA on mineral clusters has been discussed in our previous paper.[15] TEM shows that the AIO-PCDA clusters are mostly isolated with an average size of 2.6 nm (Figure 1 d–f). The presence of Fe in the cluster can be detected by energy-dispersive X-ray spectroscopy (EDX, Figure S3). SAED confirms the amorphous nature of AIO-PCDA clusters, which can also be evidenced by powder X-ray diffraction (XRD, Figure S4), indicating the lack of long-range order of a bulk solid phase formed from clusters, where PCDA ligation inhibits crystallization. Dynamic light scattering (DLS, Figure S5) and analytical ultracentrifugation (AUC) sedimentation velocity measurements (Figure S6) corroborate the small size and narrow size distribution. In solution, the size is approximately 3.5 nm (DLS, number weighted), that is, a little larger than in the dry state observed by TEM. Small angle X-ray scattering (SAXS, Figure S7) analysis of the cluster dispersion in toluene indicates the presence of fractal cylinder-like cluster aggregates with a cylinder diameter of 2.6 ± 1.2 nm and a length of 38 ± 2 nm due to the dynamic interdigitation of PCDA chains. This result is supported by a 2-dimensional spectrum analysis (2DSA)[16] performed on the AUC dataset. A plot of the frictional ratio f/f_0 versus the sedimentation coefficient (Figure S8) shows many spherical species (f/f_0 about 1), but the major species at $s = 40$ S with $f/f_0 = 1.7$ (1.6×21.9 nm) and another elongated species at $s = 15$ S with $f/f_0 = 1.6$ (1.1×12.3 nm) can also be found. Figure S9 shows that all detected species in AUC are significant aggregates of the primary unit (1678 g mol^{-1}) with molar masses of 50 000 to 600 000 g mol^{-1}.

We further employed UV/Vis, ^{1}H NMR, IR and X-ray photoelectron (XPS) spectroscopic analyses to reveal the structure of the AIO clusters (Figure S10–S13). The AIO-PCDA cluster has a well-defined core–shell structure with the chelation of Fe by *gauche* PCDA chains, and the co-existence of Fe^{2+} and Fe^{3+} was also identified. Thermal gravimetric analysis (TGA, Figure S14) allows assessing the proportion of different species in the clusters, which show an atomic ratio of [Fe]:[OH]:[H_2O] of 3.3:3.3:1 for the AIO cluster and [Fe]:[OH]:[H_2O]:[PCDA] of 4.4:8.4:2.8:1 for the AIO-PCDA cluster, respectively. Matrix-assisted laser desorption/ionization time-of-flight mass spectroscopy (MALDI-TOF MS, Figure S15) further detected the largest species to be $Fe_9O_3(OH)_{16}\cdot 6H_2O$:$(PCDA)_2$, and with it, we constructed the structure of an AIO-PCDA cluster, as shown in Figure S16. The AIO core has an approximate size of 1.1 nm (Figure S17), which is apparently smaller than the ligand-free AIO cluster (ca. 1.7 nm). The iron centers within the oxyhydroxide core are linked by oxo-bridges, and two PCDA chains attach on the core by Fe-PCDA chelation. We hypothesize that the steric effect caused by two long and mobile PCDA chains effectively hinders the further hydrolysis of AIO cores but favors cylinder-like aggregation in toluene as detected by SAXS and AUC. Despite numerous reports on very small iron oxide nanocrystals[17] or AIO particles,[11] we present herein the first examples of stabilized AIO clusters, either ligand-protected or ligand-free. We note that the simple model for the internal structure of the AIO cluster presented needs to be clarified in future work. At this point it cannot be related to reported structural models for iron (oxyhydr)oxide clusters in aqueous solutions,[4a,b,5c,18] which may also be due to the different preparation conditions and cluster compositions.

As reported for other AIOs,[11a] the AIO and AIO-PCDA clusters can be crystallized in the solid state by increasing the

temperature. Calorimetric measurements on bulk samples (Figure S18) show that the AIO and AIO-PCDA clusters crystallize at 259 and 237 °C, respectively, that is, at temperatures where the second step of water loss or OH decomposition takes place (Figure S14). Clearly, the presence of ligands promotes the crystallization of AIO owing to the improved mobility of clusters. As shown in Figure S19, thermal annealing of the AIO or AIO-PCDA clusters at 360 °C for 4 h can fully crystallize them resulting in magnetite particles that show strong magnetization (indexing of the SAED patterns in Figure S20 and Table S1). Judging from the SAED patterns, the presence of PCDA is favorable for the formation of impurity-free magnetite crystals.

To further explore the heat-induced crystallization, we annealed the AIO and AIO-PCDA clusters on TEM grids at a lower temperature of 200 °C for 24 h in N_2. Upon annealing at 200 °C, not all clusters can crystallize, but crystalline magnetite particles with a lattice spacing of 0.25 nm (corresponding to the (311) face) can be found for both AIO and AIO-PCDA clusters (Figure 2a, Figure S21). The size of magnetite particles formed via the annealing of AIO-PCDA clusters (Figure S22) ranges from 3.7 to 12.2 nm (8.8 nm on average). In the cluster aggregates, few crystalline particles can also be observed (circled region in Figure 2a, also see Figure S21,S23). In high-resolution TEM images (Figure 2b), several intermediate phases can be clearly identified. The crystalline domains are misaligned, and embedded in the amorphous phase (additional TEM image in Figure S24). Crystallization may take place directly within the AIO phase, or start within the pre-aligned domains, which are similar in size to the crystalline domains within the AIO bulk. This differs from the previously reported particle accretion mechanism in solution[5b] or the oriented attachment of nanocrystals,[19] and can be further confirmed by the observation of a developing magnetite nanocrystal from the AIO phase (Figure S25).

We demonstrate that AIO bulk particles can form from the aggregation and fusion of clusters. We frequently observed the alignment of both AIO and AIO-PCDA clusters within the bulk AIO particles (Figure 2b, Figure S21). This alignment can lead to a spacing of 0.3–0.45 nm, generating "fake" diffraction patterns upon fast Fourier transformation (FFT). Note that the clusters are not perfectly aligned as illustrated in the schematic representation (Figure 2b, inset), and the pre-aligned domains cannot be regarded as constituting, or comprising any crystalline lattices.

The coexistence of AIO bulk particles, of domains of aligned AIO and AIO-PCDA clusters, respectively, and of crystalline domains, however, does not allow determining their relation in terms of mutual precursor states, unambiguously. The bulk AIO particles can be formed from the coalescence of pre-aligned clusters, or via random cluster aggregation and coalescence. The crystalline domains, on the other hand, can emerge directly within the bulk AIO phase, or the domains of pre-aligned clusters provide the environment for the onset of crystallization. In fact, in the case of AIO-PCDA, crystallization is promoted by the enhanced mobility of the clusters, strongly suggesting that pre-aligned clusters are direct precursors to iron oxide crystals. Indeed, large-area

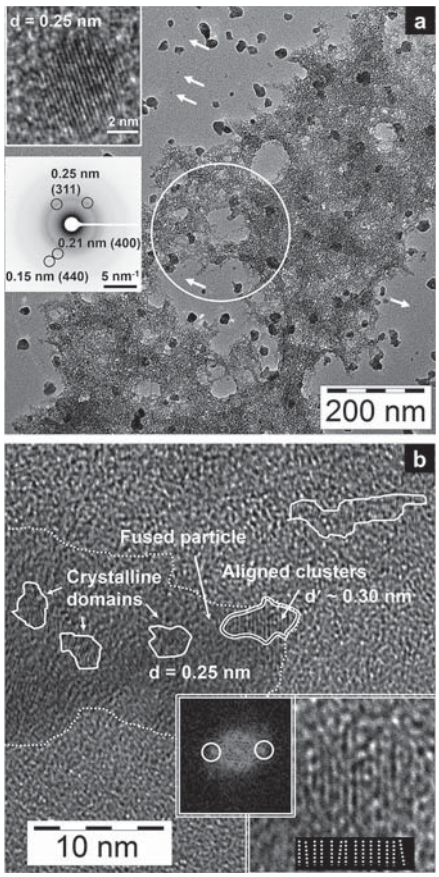

Figure 2. a) TEM image of ligand-free AIO clusters upon annealing at 200 °C for 24 h in N_2. The insets show a high-resolution TEM image of one magnetite particle (indicated by arrows) and SAED pattern of the circled region (partial crystalline). b) High-resolution TEM image of intermediate (aligned, fused, and crystalline) phases of AIO clusters upon annealing. The insets show an enlarged view of aligned clusters (double-line region, schematic cluster orientation also presented) and corresponding FFT profile showing "fake" diffraction patterns ($d' \approx 0.3$ nm).

alignment of clusters can be observed in the case of ligand-free AIO clusters (Figure S26), which points towards a kinetic inhibition of crystallization as a result of a reduced cluster mobility in the absence of the ligand, locking the process at the stage of pre-aligned clusters. All of this begs the question towards the mechanism of cluster pre-alignment. Owing to their small size, any magnetic interactions between clusters are supposed to be much weaker than thermal energy, and likely do not play a role. Thus, the alignment of clusters should be due to inherent structural characteristics. Short-range structural motifs of the clusters may involve the anisotropic binding of water,[20] or any anisotropic distributions of ions within the clusters, even without the binding of the ligand.[21] Both scenarios would give rise to the generation of dipoles that eventually underlie the self-organization into pre-aligned cluster domains. But even without any dipole formation, if a rigid bond would form between two clusters, chain formation is predicted including branching following different particle aggregation mechanisms including single-particle addition, coagulation according to Smoluchowski,

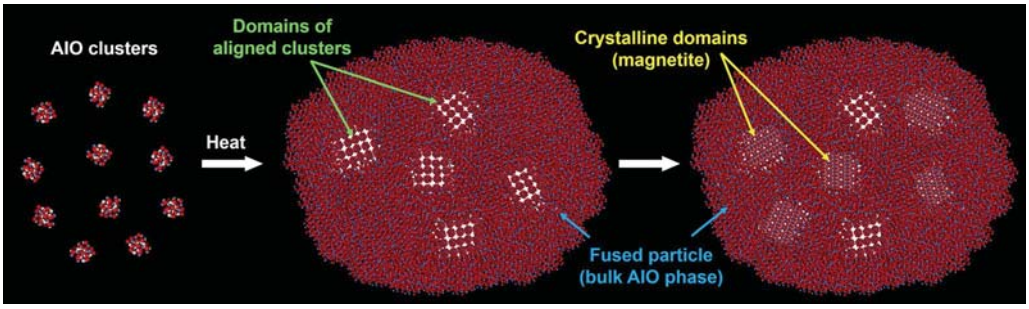

Figure 3. Schematic mechanism of the heat-induced crystallization of AIO or AIO-PCDA clusters following a non-classical, aggregation-based pathway. The top-right and bottom-left crystalline domains are formed directly from bulk AIO and the others from pre-aligned clusters.

and a maximum chain model.[22] Each of these directed aggregation scenarios would be amplified in case of directing dipoles. Note that the pre-alignment of the clusters is evident both in the solid state and in the dispersion, where chain formation is observed.

We conclude that very small AIO clusters with sizes less than 2 nm, either ligand-free or ligand-protected can be synthesized in ethanol employing a gas diffusion method. PCDA can stabilize the AIO clusters resulting in complete dispersibility in organic solvents. Although the clusters may have structures that are distinct from those of primary particles found in aqueous solutions,[5b] the synthesized clusters are direct precursors to iron oxide crystals. The non-classical, aggregation-based pathway for crystallization of calcium-based minerals[6a] also applies to the heat-induced crystallization of iron oxide. Our results suggest that domains of pre-aligned clusters pose a direct precursor stage to iron oxide crystals, whereby the presence of PCDA enhances cluster mobility, and thereby, crystallization. We hypothesize that the pre-alignment is based upon anisotropic structural features within the short-range structure of the clusters. A corresponding schematic mechanism of the cluster-based crystallization of magnetite is presented in Figure 3. We note that the alignment of small clusters cannot be discussed from the viewpoint of "oriented aggregation or attachment" (OA), as OA relies on nanocrystals. We propose that the alignment of small amorphous clusters can be explained based on simple aggregation models based on a rigid bond between two clusters[22] and dipolar interactions arising from short-range structural features, which will have to be explored in detail in future studies.

Acknowledgements

S.T.S. gratefully acknowledges the financial support from the Alexander von Humboldt Foundation and the National Science Foundation of China (NSFC; No. 21604024). D.G. is a Research Fellow of the Zukunftskolleg of the University of Konstanz, and supported by the Fonds der Chemischen Industrie. This work was also supported by the facilities in the Nanostructure Laboratory of the University of Konstanz. We thank Marina Krumova for TEM, Baohu Wu for SAXS, Martin Stärk for magnetization, Xuezhi Duan of East China University of Science and Technology for XPS analysis, and Ulrich Nowak for valuable discussions. Rose Rosenberg and Cornelia Schneider are acknowledged for performing the AUC experiments and the 2DSA analysis, respectively. We also thank the Jülich Supercomputing Centre for allocating computing time for the evaluation of the AUC data using UltraScan (Grant HKN000).

Conflict of interest

The authors declare no conflict of interest.

Keywords: aggregation · amorphous iron oxide · clusters · crystal growth · self-assembly

How to cite: *Angew. Chem. Int. Ed.* **2017**, *56*, 4042–4046
Angew. Chem. **2017**, *129*, 4100–4104

[1] R. M. Cornell, U. Schwertmann, *The iron oxides: Structure, properties, reactions, occurrences and uses*, Wiley, Hoboken, **2003**.
[2] J. Scheck, B. Wu, M. Drechsler, R. Rosenberg, A. E. S. Van Driessche, T. M. Stawski, D. Gebauer, *J. Phys. Chem. Lett.* **2016**, *7*, 3123–3130.
[3] D. Gebauer, M. Kellermeier, J. D. Gale, L. Bergström, H. Cölfen, *Chem. Soc. Rev.* **2014**, *43*, 2348–2371.
[4] a) C. M. Flynn, *Chem. Rev.* **1984**, *84*, 31–41; b) S. J. Lippard, *Angew. Chem. Int. Ed. Engl.* **1988**, *27*, 344–361; *Angew. Chem.* **1988**, *100*, 353–371; c) J. Baumgartner, D. Faivre, *Earth Sci. Rev.* **2015**, *150*, 520–530.
[5] a) J. F. Banfield, S. A. Welch, H. Zhang, T. T. Ebert, R. L. Penn, *Science* **2000**, *289*, 751–754; b) J. Baumgartner, A. Dey, P. H. H. Bomans, C. Le Coadou, P. Fratzl, N. A. J. M. Sommerdijk, D. Faivre, *Nat. Mater.* **2013**, *12*, 310–314; c) O. Sadeghi, L. N. Zakharov, M. Nyman, *Science* **2015**, *347*, 1359–1362.
[6] a) D. Gebauer, A. Völkel, H. Cölfen, *Science* **2008**, *322*, 1819–1822; b) J. J. De Yoreo, P. U. P. A. Gilbert, N. A. J. M. Sommerdijk, R. L. Penn, S. Whitelam, D. Joester, H. Zhang, J. D. Rimer, A. Navrotsky, J. F. Banfield, A. F. Wallace, F. M. Michel, F. C. Meldrum, H. Cölfen, P. M. Dove, *Science* **2015**, *349*, 6247; c) H. Cölfen, M. Antonietti, *Mesocrystals and nonclassical crystallization*, Wiley, Chichester, **2008**.
[7] a) V. M. Yuwono, N. D. Burrows, J. A. Soltis, R. L. Penn, *J. Am. Chem. Soc.* **2010**, *132*, 2163–2165; b) D. Li, M. H. Nielsen, J. R. I. Lee, C. Frandsen, J. F. Banfield, J. J. De Yoreo, *Science* **2012**, *336*, 1014–1018.
[8] C. Frandsen, B. A. Legg, L. R. Comolli, H. Zhang, B. Gilbert, E. Johnson, J. F. Banfield, *CrystEngComm* **2014**, *16*, 1451–1458.

[9] a) H. Cölfen, M. Antonietti, *Angew. Chem. Int. Ed.* **2005**, *44*, 5576 – 5591; *Angew. Chem.* **2005**, *117*, 5714 – 5730; b) M. Niederberger, H. Cölfen, *Phys. Chem. Chem. Phys.* **2006**, *8*, 3271 – 3287.
[10] S. Weiner, I. Sagi, L. Addadi, *Science* **2005**, *309*, 1027 – 1028.
[11] a) L. Machala, R. Zboril, A. Gedanken, *J. Phys. Chem. B* **2007**, *111*, 4003 – 4018; b) X. Cao, Y. Koltypin, G. Katabi, R. Prozorov, I. Felner, A. Gedanken, *J. Mater. Chem.* **1997**, *7*, 1007 – 1009; c) R. V. Kumar, Y. Koltypin, Y. S. Cohen, Y. Cohen, D. Aurbach, O. Palchik, I. Felner, A. Gedanken, *J. Mater. Chem.* **2000**, *10*, 1125 – 1129; d) K. V. P. M. Shafi, A. Ulman, X. Yan, N.-L. Yang, C. Estournès, H. White, M. Rafailovich, *Langmuir* **2001**, *17*, 5093 – 5097; e) H. Cohen, A. Gedanken, Z. Zhong, *J. Phys. Chem. C* **2008**, *112*, 15429 – 15438; f) L. Wang, X. Zhang, S. Wang, Y. Li, B. Qian, X. Jiang, G. Yang, *Powder Technol.* **2014**, *256*, 499 – 505; g) Z. Wang, L. Zhao, P. Yang, Z. Lv, H. Sun, Q. Jiang, *Chem. Eng. J.* **2014**, *235*, 231 – 235.
[12] a) H. S. Lee, T. H. Ha, K. Kim, *Mater. Chem. Phys.* **2005**, *93*, 376 – 382; b) S.-F. Chen, H. Cölfen, M. Antonietti, S.-H. Yu, *Chem. Commun.* **2013**, *49*, 9564 – 9566; c) S. Sun, D. M. Chevrier, P. Zhang, D. Gebauer, H. Cölfen, *Angew. Chem. Int. Ed.* **2016**, *55*, 12206 – 12209; *Angew. Chem.* **2016**, *128*, 11939 – 11943.
[13] P. Layrolle, A. Lebugle, *Chem. Mater.* **1994**, *6*, 1996 – 2004.
[14] M. Hajir, R. Graf, W. Tremel, *Chem. Commun.* **2014**, *50*, 6534 – 6536.
[15] S. Sun, D. Gebauer, H. Cölfen, *Chem. Sci.* **2017**, *8*, 1400 – 1405.
[16] E. Brookes, W. Cao, B. Demeler, *Eur. Biophys. J.* **2010**, *39*, 405 – 414.
[17] a) J. Park, K. An, Y. Hwang, J.-G. Park, H.-J. Noh, J.-Y. Kim, J.-H. Park, N.-M. Hwang, T. Hyeon, *Nat. Mater.* **2004**, *3*, 891 – 895; b) J. Park, E. Lee, N.-M. Hwang, M. Kang, S. C. Kim, Y. Hwang, J.-G. Park, H.-J. Noh, J.-Y. Kim, J.-H. Park, T. Hyeon, *Angew. Chem. Int. Ed.* **2005**, *44*, 2872 – 2877; *Angew. Chem.* **2005**, *117*, 2932 – 2937.
[18] a) F. M. Michel, V. Barrón, J. Torrent, M. P. Morales, C. J. Serna, J.-F. Boily, Q. Liu, A. Ambrosini, A. C. Cismasu, G. E. Brown, *Proc. Natl. Acad. Sci. USA* **2010**, *107*, 2787 – 2792; b) H. Zhang, G. A. Waychunas, J. F. Banfield, *J. Phys. Chem. B* **2015**, *119*, 10630 – 10642; c) J.-P. Jolivet, E. Tronc, C. Chanéac, *C. R. Geosci.* **2006**, *338*, 488 – 497.
[19] H. Zhang, J. J. De Yoreo, J. F. Banfield, *ACS Nano* **2014**, *8*, 6526 – 6530.
[20] a) M. Farhadi-Khouzani, D. M. Chevrier, P. Zhang, N. Hedin, D. Gebauer, *Angew. Chem. Int. Ed.* **2016**, *55*, 8117 – 8120; *Angew. Chem.* **2016**, *128*, 8249 – 8252; b) C. Rodriguez-Navarro, K. Kudłacz, Ö. Cizer, E. Ruiz-Agudo, *CrystEngComm* **2015**, *17*, 58 – 72.
[21] A. Schreiber, M. C. Huber, H. Cölfen, S. M. Schiller, *Nat. Commun.* **2015**, *6*, 6705.
[22] D. N. Sutherland, *Nature* **1970**, *226*, 1241 – 1242.